Unimolecular and Photoinduced Dissociations of Aromatic $C_8H_{10}^{+\bullet}$ Molecular Ions

Yeon Ho Kim,[†] Joong Chul Choe,[‡] and Myung Soo Kim*[,†]

National Creative Research Initiative for Control of Reaction Dynamics and School of Chemistry, Seoul National University, Seoul 151-742, Korea, and Department of Chemistry, University of Suwon, Suwon 440-600, Korea

Received: December 7, 2000; In Final Form: March 12, 2001

Production of $C_7H_7^+$ in the unimolecular and photoinduced dissociations of ethylbenzene; methylcycloheptatriene; and *o*-, *m*-, and *p*-xylene ions has been investigated using mass-analyzed ion kinetic energy spectrometry. Both the benzylium and tropylium ions were produced near the reaction threshold, whereas only the benzylium ion was observed at higher internal energy achieved by photoabsorption. Experimental data suggest that interconversion between ethylbenzene and methylcycloheptatriene ions occurs more rapidly than their dissociations near the reaction threshold, whereas xylene ions undergo rate-determining isomerization to the methylcycloheptatriene structure, and dissociation occurs from the ethylbenzene/methylcycloheptatriene ion mixture. The processes occurring at higher internal energy are quite similar, except that the tropylium channel cannot compete against the benzylium channel because either the ethylbenzene ion-to-methylcycloheptatriene ion conversion or the dissociation of the methylcycloheptatriene ion to the tropylium ion is slower than the direct dissociation of the ethylbenzene ion. The above mechanistic picture is in disagreement with the prediction of a dynamic model reported previously. A series of investigations performed for the production of $C_7H_7^+$ from alkylbenzene ions shows an interesting trend of increasing benzylium production with the increase in the total number of carbon atoms in the alkyl substituents.

1. Introduction

Production of $C_7H_7^+$ from various molecular ions, alkylbenzene ions in particular, has been the subject of numerous experimental and theoretical studies in the field of gas-phase ion chemistry.[1−14] The main focus of these studies has been the isomeric compositions of the $C_7H_7^+$ ions generated and the associated mechanistic pathways. Among the several possible isomeric forms of $C_7H_7^+$, the benzylium (Bz^+, **1**) and tropylium (Tr^+, **2**) ions have been found to be the most important products in the dissociation of alkylbenzene ions near the threshold energy.

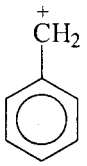

1

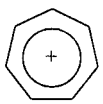

2

In the case of the toluene ion, both of these are known[1−3] to be produced: Bz^+ via simple bond cleavage and Tr^+ via isomerization to and simple bond cleavage from the cycloheptatriene ion. It is also known that interconversion between toluene and cycloheptatriene ions is rapid near the threshold for hydrogen loss.[1−3] On the other hand, Bz^+ was found to be produced preferentially from *n*-propyl-[10] and *n*-butylbenzene[11] ions. A molecular orbital calculation and an estimate of the rate-energy relations for the dissociation of the *n*-propylbenzene ion showed that isomerization to the ethylcycloheptatriene ion could not compete effectively with the direct cleavage to Bz^+.[10] This was because the isomerization barrier height, which was lower than that for direct cleavage in the toluene ion case, is comparable to the latter in the *n*-propylbenzene ion case. A similar argument is expected to hold for the dissociation of alkylbenzene ions with larger alkyl chains.

Not mentioned so far is the dissociation of the aromatic $C_8H_{10}^{+\bullet}$ ions, namely, ethylbenzene ($EB^{+\bullet}$); 7-methylcycloheptatriene ($MC^{+\bullet}$); and *o*-, *m*-, and *p*-xylene ($pXL^{+\bullet}$, etc.) ions, which have been widely investigated also. Williams and co-workers observed that the average kinetic energy releases in the metastable ion decompositions (MIDs) of $EB^{+\bullet}$ and $MC^{+\bullet}$ were essentially the same and postulated that isomerization between these structures must be rapid and that both $EB^{+\bullet}$ and $MC^{+\bullet}$ dissociate to Tr^+.[12] Grotemeyer and Grützmacher carried out an extensive mass spectrometric study of these ions using ^{13}C- and D-labeled compounds.[13] Also performed were semi-empirical molecular orbital calculations for structures along various reaction paths. It was found that $Tr^+ + CH_3^\bullet$ was lower (by ∼0.5 eV) in energy than $Bz^+ + CH_3^\bullet$ and, hence, assumed to be the dominant dissociation channel, in agreement with Williams and co-workers. On the other hand, analysis of the product ion structure utilizing chemical reactivity of Bz^+ with toluene in an ion cyclotron resonance spectrometer by Ausloos[14] and collision-induced dissociation study by Holmes and co-workers[2] suggested that both Tr^+ and Bz^+ were produced near the threshold. Considering the trend described above that both Bz^+ and Tr^+ are produced from the toluene ion while *n*-propyl- and *n*-butylbenzene ions produce Bz^+ only, it is likely that $EB^{+\bullet}$ and $MC^{+\bullet}$ produce Bz^+ in addition to Tr^+.

In this work, the kinetic energy release distributions (KERDs) for the unimolecular dissociations of $EB^{+\bullet}$; $MC^{+\bullet}$; and *o*-, *m*-,

* To whom correspondence should be addressed.
[†] Seoul National University.
[‡] University of Suwon.

10.1021/jp0044072 CCC: $20.00
Published on Web 05/22/2001

and *p*-xylene ions near the threshold, or MID, were analyzed in detail to find evidence for the production of Bz^+ and Tr^+. This approach is advantageous in the sense that KERD depends on the dissociation step only and is not affected by isomerization processes which may occur before or after the dissociation. Photodissociation (PD) kinetics experiments were also performed to gain further information on the isomerization processes.

2. Experimental Section

A double focusing mass spectrometer with reversed geometry (VG Analytical model ZAB-E) modified for PD study was used.[15] Samples were introduced into the ion source via a septum inlet and ionized by 70 eV electron ionization or by charge exchange ionization using CS_2 as the reagent gas. Molecular ions generated in the ion source at 180 °C in electron ionization or at 140 °C in charge exchange ionization were accelerated to 8 keV and mass-separated by the magnetic sector. Then, the translational kinetic energy of a product ion generated in the second field-free region of the instrument was analyzed by the electric sector. This is called the mass-analyzed ion kinetic energy spectrometry (MIKES). Two different modes of dissociation of the molecular ions, MID and PD, were investigated. To generate the molecular ions for the MID study, 70 eV electron ionization was used. For the PD study, the charge exchange ionization was used.

The PD technique developed in this laboratory for the study of ion dissociation dynamics was described in detail previously.[15] Briefly, the molecular ion beam was crossed perpendicularly by a laser beam inside an electrode assembly located near the intermediate focal point of the instrument. The 514.5 and 488.0 nm lines of an argon ion laser (Spectra Physics model 164-09) were used for PD of the molecular ions. A MIKE spectrum for PD, or a PD-MIKE spectrum, is often contaminated by contributions from the same reactions occurring unimolecularly (MID) or by collision of the precursor ions with the residual gas. Hence, phase-sensitive detection was adopted to record a MIKE spectrum originating only from PD. To improve the quality of MIKE spectra, signal averaging was carried out for repetitive scans. Errors quoted in this work were estimated from several duplicate experiments at the 95% confidence limit.

7-Methylcycloheptatriene was synthesized according to the methods of Harrison et al.[16] and Conrow[17] and purified by distillation. Its structure was identified using the ^1H NMR[18] and normal mass spectra.[19] Other compounds were purchased from Aldrich and used without further purification.

3. Results and Discussion

For dissociation, both MID and PD, of all of the $C_8H_{10}^{+\bullet}$ isomers investigated in this work, methyl loss was the dominant channel (>95% of the total). Scheme 1 shows possible pathways for isomerization and dissociation of $C_8H_{10}^{+\bullet}$ isomers (to be confirmed experimentally in this work). Dissociation of a xylene ion to a tolyl ion is not thought to be important near the reaction threshold (to be explained). The pathways for the ortho and meta isomers of the xylene ion are likely to be similar to the para case, as will be confirmed later. Throughout the work, the results for the para isomer will be discussed almost exclusively.

Energetics. Thermochemical data[20−24] for the important neutral and ionic species relevant to the present study are listed in Table 1. Because the thermochemical data for $MC^{+\bullet}$ is not available in the literature, its energy relative to $EB^{+\bullet}$ was estimated by comparing energies of these ions obtained by electronic structure calculations at the HF/6-31G** level and also at the B3LYP/6-31G** level of the density-functional theory.[25] These are 77.2 and 60.8 kJ mol^{-1} at the HF/6-31G** and B3LYP/6-31G** levels, respectively, which are larger than 42 kJ mol^{-1} at the MNDO level reported by Grotemeyer and Grützmacher.[13] The energy of the products $Tr^+ + CH_3^\bullet$ was calculated at the same levels. The transition state for the reaction $MC^{+\bullet} \rightarrow Tr^+ + CH_3^\bullet$ was also found. The height of the reverse barrier was 40 and 1 kJ mol^{-1} respectively at the HF/6-31G** and B3LYP/6-31G** levels. In our previous study on the toluene ion,[8] the reverse barrier in the dissociation of the cycloheptatriene ion to $Tr^+ + H^\bullet$ calculated at the HF level, 27.0 kJ mol^{-1}, was in excellent agreement with the G2 result of 26.1 kJ mol^{-1}, whereas the B3LYP/6-31G** calculation[26] resulted in a smaller barrier (11.1 kJ mol^{-1}). More importantly, a classical trajectory calculation on the HF potential-energy surface resulted in KERD that was in good qualitative agreement with the experimental one.[8] Assuming that the same trend holds for the present system, the HF/6-31G** result will be adopted here for the $MC^{+\bullet} \rightarrow Tr^+ + CH_3^\bullet$ part of the potential-energy diagram. Figure 1 shows the potential-energy diagram for the reaction pathways in Scheme 1. The electronvolt was used as the energy unit rather than kilojules per mole for ease of comparison with the experimental data. The transition states connecting $C_8H_{10}^{+\bullet}$ isomers could not be located beyond the semiempirical levels, and their energies drawn as dashed line in the figure have no quantitative meaning.

SCHEME 1

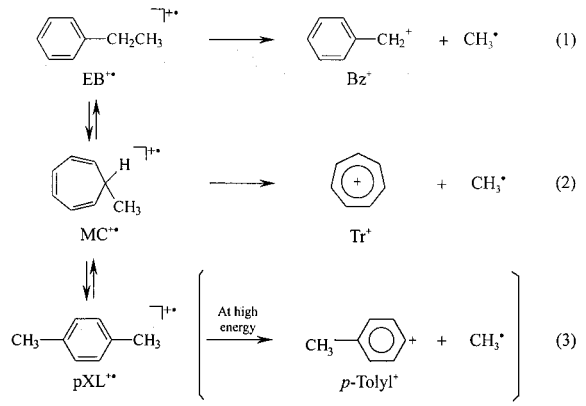

TABLE 1: Energetics Data

species[a]	$\Delta H^0_{f,298K}$ (kJ mol^{-1})	$\Delta H^0_{f,0K}$[b] (kJ mol^{-1})	calculated energy[c] (kJ mol^{-1}) HF	B3LYP	IE (eV)
EB	29.3[d]	60.6			8.77[e]
pXL	18.0[d]	45.5			8.44[e]
$EB^{+\bullet}$	874[d]	907	0	0	
$pXL^{+\bullet}$	832[d]	860	−33.8	−47.3	
$MC^{+\bullet}$			77.2	60.8	
TS			160.7	132.3	
Bz^+	907[g]	926[g]			
p-tolyl$^+$	1074[f]	1094			
$CH_3^\bullet$	145.8[d]	149.0			
$Tr^+ + CH_3^\bullet$			120.6	131.2	

[a] Abbreviations: EB (ethylbenzene), pXL (*p*-xylene), MC (7-methylcycloheptatriene), Bz^+ (benzylium ion), Tr^+ (tropylium ion), TS (transition state for $MC^{+\bullet} \rightarrow Tr^+ + CH_3^\bullet$). [b] Estimated from 298 K data as described in ref 20. [c] Energy at the zero point referred to that of $EB^{+\bullet}$. [d] Taken from ref 21. [e] Taken from ref 22. [f] Taken from ref 23. [g] Taken from ref 24.

Kinetic Energy Release Distribution (KERD). ***Unimolecular Dissociation.*** Figure 2a shows the MIKE spectral profiles for the unimolecular dissociation ($CH_3^\bullet$ loss) of $EB^{+\bullet}$ and $pXL^{+\bullet}$

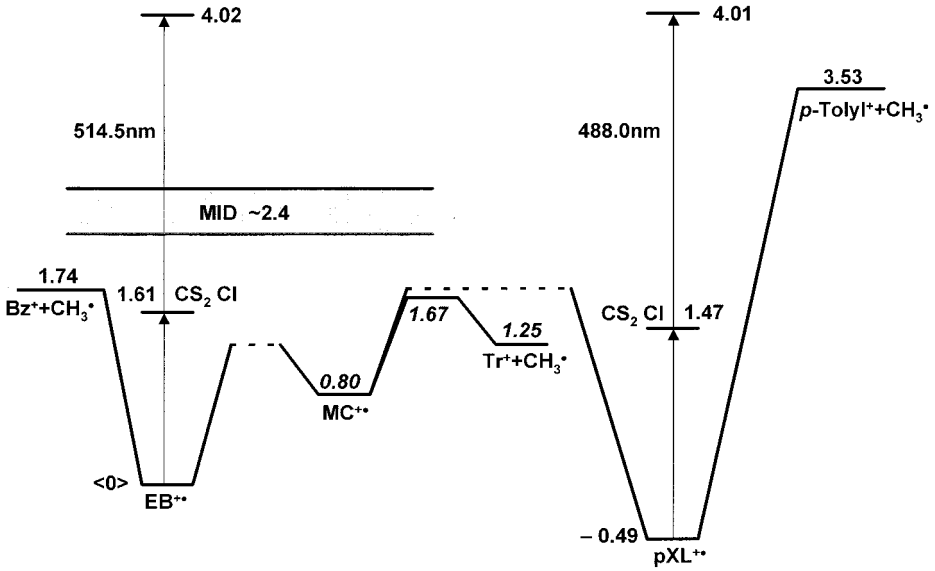

Figure 1. A schematic potential-energy diagram for the production of $C_7H_7^+$ from $C_8H_{10}^{+\bullet}$ isomers. The numbers denote the energy in eV referred to the energy minimum of ethylbenzene ion ($EB^{+\bullet}$). The energies of $EB^{+\bullet}$, *p*-xylene ion ($pXL^{+\bullet}$), and some products were estimated from the thermochemical data listed in Table 1. The energies estimated from the molecular orbital calculations at the HF/6-31G** level are denoted by italics. Dashed lines indicate unidentified transition states. The energies for the photoexcited molecular ions are shown. The internal energy range for MID of $EB^{+\bullet}$ and methylcycloheptatriene ($MC^{+\bullet}$) are also indicated. The energy corresponding to MID of $pXL^{+\bullet}$ is thought to be slightly higher than this.

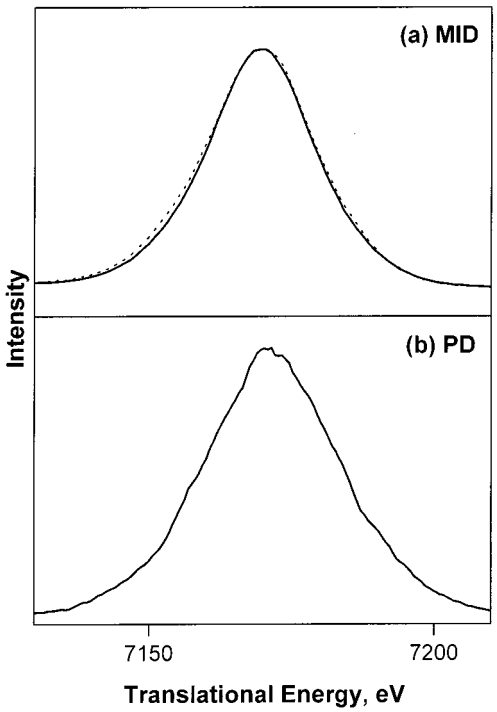

Figure 2. (a) MID-MIKE profiles for the production of $C_7H_7^+$ from $EB^{+\bullet}$ (—) and $pXL^{+\bullet}$ (- - -). (b) PD-MIKE profile for the production of $C_7H_7^+$ from $EB^{+\bullet}$ at 514.5 nm.

recorded with the electrode assembly floated at 2.0 kV. The corresponding MIKE profile for $MC^{+\bullet}$ was essentially identical to that of $EB^{+\bullet}$ and those for the *o*- and *m*-xylene ions to that of $pXL^{+\bullet}$ and are not shown. As can be seen in the figure, the spectral profiles for $EB^{+\bullet}$ and $pXL^{+\bullet}$ are very similar also, with the $pXL^{+\bullet}$ profile being slightly broader. The method developed in this laboratory[27] to evaluate KERD from a MIKE profile introduces some fluctuation originating from high-frequency noise in the spectrum and may not be adequate to see the tiny difference in KERDs of the two reactions. In this work, we recorded the MIKE profiles with the parent ion resolution of ~2.8 eV such that deconvolution of the instrumental broadening was not needed. Because the kinetic energy releases were quite small, such that the instrumental discrimination effect was not important,[28] the method developed by Holmes and Osborne[29] was used to evaluate KERDs by fitting the MIKE profiles to the symmetric function

$$y = e^{-ax^2}(1 + b_2x^2 + b_4x^4 + b_6x^6) \quad (4)$$

Here, y is the MIKE profile normalized at the peak height and x is the translational energy referred to the center of the profile. The KERDs thus obtained from the MIKE profiles in Figure 2a are shown in Figure 3 parts a and b. It is to be noted that KERDs in these figures display very similar pattern. In fact, the main purpose of using the noise-free approach in the profile analysis was more to demonstrate the striking similarity in KERDs obtained from all of the five precursor ions than to see the minor difference between KERDs.

Also noticeable in Figure 3 parts a and b is that these KERDs are clearly bimodal, namely, that two different dissociation processes are involved. The production of tolyl ions is much more endothermic than the production of Bz^+ and Tr^+ and can be neglected for dissociation near the threshold (see Figure 1). Then, it is likely that the latter two channels, namely, reactions 1 and 2, are involved in the dissociation step. Because the production of Tr^+ is associated with some reverse barrier, whereas that of Bz^+ is a simple bond cleavage occurring without a reverse barrier, it is reasonable to relate the former to the features appearing at higher energy parts of KERDs and the latter to those at lower energy. The same assignments were made previously for bimodal KERDs observed in the dissociation of other aromatic ions.[8, 30]

An experimental KERD appearing bimodal can be separated into two components using the surprisal analysis.[31] The surprisal factor I, a measure of the extent of deviation of a distribution from a prior expectation, is defined as follows:

$$I(T) = -\ln[n(T)/n_0(T)] \quad (5)$$

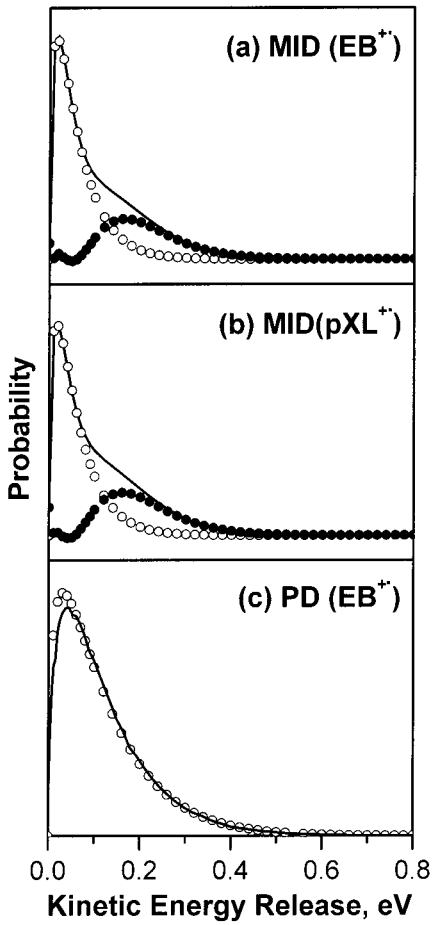

Figure 3. KERDs of $C_7H_7^+$ generated by unimolecular dissociation (MID) of (a) $EB^{+\bullet}$ and (b) $pXL^{+\bullet}$ are shown as solid curves. Bz^+ and Tr^+ components in MID-KERDs separated by the surprisal analysis are shown as open (○) and solid (●) circles, respectively. KERD in PD of $EB^{+\bullet}$ at 514.5 nm is shown in (c) as a solid line together with the KERD calculated with the phase space theory (open circles).

Here, $n(T)$ and $n_0(T)$ represent the experimental and expected KERDs, respectively. It is usual to use a KERD calculated by statistical theories as $n_0(T)$. Because the kinetic energy release distribution in the production of Bz^+, which is a simple bond cleavage occurring without reverse barrier, is expected to be well described by statistical theories, we calculated this with the phase space theory (PST)[32] as follows and used it as $n_0(T)$:

$$n(T;J,E) \propto \int_{R_m}^{E-E_0-T} \rho(E - E_0 - R)P(T,J,R)\,\mathrm{d}R \qquad (6)$$

Here, $n(T;J,E)$ is the KERD at the angular momentum J and the internal energy E. The root-mean-square average J evaluated at the ion source temperature was used. ρ and P are product vibrational and angular momentum state densities, respectively. R is the product rotational energy and R_m is its minimum. E_0, the reaction critical energy, was set equal to the reaction endoergicity at 0 K, assuming a completely loose transition state. Its best estimate from the thermochemical data listed in Table 1 was 1.74 eV. Other molecular parameters used for the calculation are listed in Table 2. The internal energy of $EB^{+\bullet}$ undergoing MID can be estimated reliably when an accurate rate-energy relation is known.[33] Because this is not available, a rough estimation was made based on the rate constant data obtained by PD of $EB^{+\bullet}$ (see below) in this work. It was about 2.4 eV. The surprisal plot for the methyl loss of

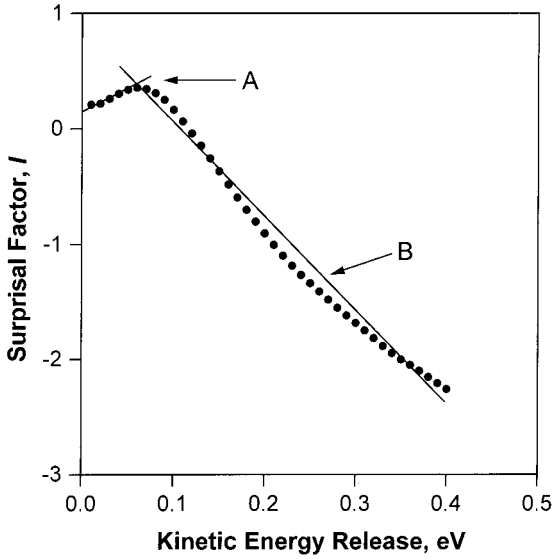

Figure 4. Surprisal plot for the experimental MID-KERD in Figure 3a. The slopes of the lines A and B are 3.1 ± 1.0 and −8.1 ± 0.9, respectively.

TABLE 2: Molecular Parameters Used in the Calculations of KERDs and Thermal Energy Distributions[a]

	vibrational frequencies (cm^{-1})
$pXL^{+\bullet}$	56, 57, 104, 241, 275, 345, 355, 392, 461, 511, 618, 653, 759, 793, 812, 894, 965, 973, 979, 1002, 1009, 1013, 1098, 1117, 1158, 1180, 1256, 1260, 1364, 1369, 1370, 1401, 1421, 1421, 1428, 1435, 1464, 1586, 2844, 2844, 2899, 2899, 2959, 2959, 3011, 3013, 3030, 3031
$EB^{+\bullet}$	41, 103, 198, 239, 339, 349, 394, 420, 488, 620, 715, 769, 770, 791, 890, 912, 918, 949, 966, 996, 998, 1003, 1049, 1105, 1156, 1162, 1200, 1276, 1277, 1312, 1350, 1379, 1407, 1443, 1446, 1466, 1479, 1591, 2863, 2880, 2924, 2941, 2947, 3016, 3020, 3024, 3032, 3036
Bz^+	163, 337, 342, 407, 510, 582, 611, 628, 778, 782, 843, 946, 963, 976, 1000, 1012, 1046, 1089, 1112, 1134, 1157, 1307, 1311, 1326, 1420, 1452, 1540, 1547, 1583, 2975, 3011, 3015, 3017, 3036, 3039, 3067
$CH_3^\bullet$	304, 1365, 1365, 2911, 3072, 3072

	rotational constants (cm^{-1})			polarizability (10^{-24} cm^3)
$EB^{+\bullet}$	0.1494	0.0490	0.0405	
Bz^+	0.1807	0.0939	0.0618	
$CH_3^\bullet$	9.3002	9.3002	4.6501	9.25

[a] HF/6-31G** results. All frequencies are scaled by 0.89.[33]

$EB^{+\bullet}$ thus obtained is shown in Figure 4. The fact that the surprisal plot consists of two nearly straight lines is the clear indication that the experimental KERD is bimodal. The small surprisal at small kinetic energy release (T = 0∼0.1 eV) means that the component with small kinetic energy release is well-explained by statistical dissociation to $Bz^+ + CH_3^\bullet$ via a loose transition state. The experimental KERD was separated into two components, small and large KER components, using the method described previously.[30] The results are shown in Figure 3 parts a and b for the methyl losses of $EB^{+\bullet}$ and $pXL^{+\bullet}$. The large KER components start at ∼0.05 eV (5 kJ mol^{-1}), indicating a nonzero reverse barrier associated with this reaction, probably via $MC^{+\bullet} \rightarrow Tr^+ + CH_3^\bullet$. Because the reverse barrier will not be entirely released as the translation energy of the products, one cannot estimate the magnitude of the reverse barrier from the experimental data. From the shapes of KERD for the large KER components in Figure 3, however, one may take 5 kJ mol^{-1} as the lower limit for the reverse barrier. This

TABLE 3: Small and Large Kinetic Energy Release (KER) Components in the Unimolecular Dissociation (MID) of Ethylbenzene ($EB^{+\bullet}$) and *p*-Xylene ($pXL^{+\bullet}$) Ions Separated by Surprisal Analysis

	$EB^{+\bullet}$		$pXL^{+\bullet}$	
	small KER	large KER	small KER	large KER
fraction (%)	66	34	67	33
average KER (eV)	0.050	0.203	0.056	0.211

is certainly larger than 1 kJ mol^{-1} obtained in the B3LYP/6-31G** calculation. Of course, this does not mean that the experimental results are compatible with the reverse barrier (40 kJ mol^{-1}) obtained in the HF/6-31G** calculation. In the case of the dissociation of $C_8H_{10}^{+\bullet}$ generated from ethylbenzene and methylcycloheptatriene, the small KER component was 66% of the total. More importantly, the fact that KERDs for these reactions are identical within the experimental error limit indicates that the isomerization between $EB^{+\bullet}$ and $MC^{+\bullet}$ occurs rapidly at the internal energy needed for the observation of MID. This is in agreement with the postulation by Williams and co-workers,[12] even though the fact that the Bz^+ channel is present is in conflict with the Tr^+-only postulation suggested by these investigators.

A surprisal analysis for the dissociation of $pXL^{+\bullet}$ gives nearly the same results as for $EB^{+\bullet}$. The fractions of the small and large KER components and the average kinetic energy releases for each component for dissociations of $EB^{+\bullet}$ and $pXL^{+\bullet}$ are compared in Table 3. Each value in the table will depend on the experimental condition and may not be accurate enough. However, these were obtained through the same treatment of experimental data obtained at the identical condition and have good precision in a relative sense. Hence, it seems to be safe to say that the Bz^+/Tr^+ ratios are essentially the same for dissociations of $EB^{+\bullet}$ and $pXL^{+\bullet}$ and that $pXL^{+\bullet}$ dissociates via the same channels as $EB^{+\bullet}$ but at an internal energy a few to several tenths of an electronvolt higher than that of $EB^{+\bullet}$. This is in agreement with the postulation by Williams and co-workers[12] that the isomerization of $pXL^{+\bullet}$ to $MC^{+\bullet}$ is the rate-determining step in MID of $pXL^{+\bullet}$.

According to the semiempirical calculation by Grotemeyer and Grützmacher, the isomerization rate constant for $MC^{+\bullet} \rightarrow pXL^{+\bullet}$ was much faster than that for $MC^{+\bullet} \rightarrow EB^{+\bullet}$.[13] On the basis of the calculated rate constants, it was concluded that $pXL^{+\bullet}$ and $MC^{+\bullet}$ interconverted freely, whereas $EB^{+\bullet}$ and $MC^{+\bullet}$ did not and that all these ions dissociated to $Tr^+ + CH_3^\bullet$. The present experimental observation of the $Bz^+ + CH_3^\bullet$ channel and of near constancy of the Bz^+/Tr^+ ratio for the dissociations from all of the precursor ions are in conflict with the above conclusions. Rather, the isomerization between $MC^{+\bullet}$ and $EB^{+\bullet}$ seems to be rapid at the metastable energy window. In the case of $pXL^{+\bullet}$, isomerization to $MC^{+\bullet}$ is the rate-determining step, followed by rapid isomerization to $EB^{+\bullet}$ and dissociation from the $MC^{+\bullet}/EB^{+\bullet}$ mixture to Tr^+ and Bz^+. It was mentioned earlier that all of the three isomers of the xylene ions display essentially the same MIKE profiles. Williams and co-workers suggested that xylene isomeric ions undergo a rate-determining isomerization via transition states which have very similar energies or via the same transition state to $MC^{+\bullet}$ structure.[12] Results from the detailed analysis of the KERD data made here support this suggestion.

Photodissociation. The MIKE spectrum for PD of $EB^{+\bullet}$ was recorded under the similar experimental condition as for MID, namely, with the electrode assembly floated at 2.0 kV. The MIKE profile for the methyl loss in PD, namely, the PD-MIKE profile, of $EB^{+\bullet}$ at 514.5 nm is shown in Figure 2b and the KERD evaluated from this profile is in Figure 3c. Unlike its MID counterpart (Figure 3a), the KERD in PD looks monotonic and indicates that the Tr^+ channel does not contribute significantly in this case. To see if the Bz^+ channel is the main pathway, the KERD was calculated for this channel using phase space theory. Because the molecular ion for PD was generated by charge exchange with $CS_2^{+\bullet}$, its internal energy after photoexcitation can be estimated as follows:

$$E = \mathrm{RE} - \mathrm{IE} + E_{\mathrm{th}} + h\nu \qquad (7)$$

Here, RE and IE are the recombination energy of $CS_2^{+\bullet}$ and the ionization energy of ethylbenzene, the best literature values of which are 10.07[35] and 8.77[22] eV (971.6 and 846 kJ mol^{-1}), respectively. E_{th} is the thermal internal energy at the ion source temperature of 140 °C. Its average, 0.31 eV, was calculated using the molecular parameters in Table 2.[15] The average internal energy of $EB^{+\bullet}$ photoexcited at 514.5 nm estimated with eq 7 is 4.02 eV. The PST-KERD for PD at 514.5 nm is shown in Figure 3c, which agrees well with the experimental KERD, indicating that the Bz^+ channel is the main pathway, as assumed. Namely, the Bz^+ channel is the dominant pathway at ~2.3 eV above the threshold (PD), even though the Tr^+ channel can compete effectively at several tenths of an eV above the threshold (MID). We could not perform a PD experiment for $MC^{+\bullet}$ with well-defined internal energy. For example, most of $MC^{+\bullet}$ generated by charge exchange with $CS_2^{+\bullet}$ fragmented in the ion source.

We recorded the PD-MIKE spectrum of $pXL^{+\bullet}$, and other xylene isomeric ions also, at 488.0 nm (not shown) and calculated the KERD. These were essentially the same as the PD-KERD for $EB^{+\bullet}$ at 514.5 nm (Figure 3c) within the error limit. According to Figure 1, production of tolyl ions (reaction 3) is energetically possible in PD of $C_8H_{10}^{+\bullet}$ ions. Its PD rate constant was estimated roughly with the Rice−Ramsperger−Kassel−Marcus (RRKM) theory,[34] which was less than 10^{-2} s^{-1}. Such a slow process cannot be detected at all with the present apparatus. In fact, the PD rate constant of $pXL^{+\bullet}$ determined experimentally (see below) was larger than the above by several orders of magnitude. This rules out the possibility of the tolyl ion production.

As shown in Figure 1, the energy available in PD of $pXL^{+\bullet}$ in the production of $Bz^{+\bullet} + CH_3^\bullet$ at 488.0 nm, 2.27 eV, is almost the same as that of $EB^{+\bullet}$ at 514.5 nm, 2.28 eV. Then, essentially identical KERDs in PD of $EB^{+\bullet}$ and $pXL^{+\bullet}$ at nearly the same internal energy suggest that PD of $pXL^{+\bullet}$ also generates $Bz^+ + CH_3^\bullet$, possibly via the same mechanism as in MID. Grotemeyer and Grützmacher calculated the potential-energy diagram for the "H ring-walk" mechanism of $pXL^{+\bullet}$ using the MNDO method (Scheme 2).[13]

They also calculated the overall rate-energy relation for the production of $Bz^+ + CH_3^\bullet$ via this mechanism and suggested that this pathway be dominant at the internal energy higher than the metastable window. It is difficult to judge which of the two mechanisms, $pXL^{+\bullet} \rightarrow MC^{+\bullet} \rightarrow EB^{+\bullet} \rightarrow Bz^+ + CH_3^\bullet$ (mechanism 1) or the "H ring-walk" mechanism (mechanism 2), are responsible for the methyl loss of $pXL^{+\bullet}$ in PD. In both mechanisms, the final steps, which determine the kinetic energy release, are simple bond cleavages to $Bz^+ + CH_3^\bullet$. If both of these proceed statistically, as was confirmed for mechanism 1 (Figure 3c), one would expect similar KERD regardless of the mechanism. Even though the rate-energy data calculated at the MNDO level favors mechanism 2, we do not have much faith in the reliability of the rate-energy data calculated with the MNDO results. This is because they are not compatible with

SCHEME 2

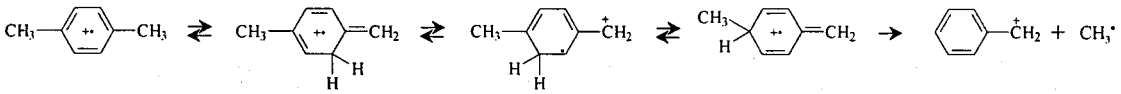

the present experimental results as mentioned above. Even though we attempted to reproduce the reaction pathways at higher levels and to obtain more reliable rate-energy data, we could not locate most of the transition states. However, we could locate the transition state for the final step of the dissociation via the "H ring-walk" at the HF/6-31G** level and found the presence of the reverse barrier of 0.07 eV. The presence of the reverse barrier in this simple bond cleavage reaction must be due to the aromatic stabilization of the product Bz^+, just as in $MC^{+\bullet} \rightarrow Tr^+ + CH_3^\bullet$. Then, if PD of $pXL^{+\bullet}$ proceeds solely via this pathway, one would expect a nonstatistical-looking KERD with small probability near zero kinetic energy release, in contrast with the present experimental result. Or, if PD of $pXL^{+\bullet}$ proceeds via mechanism 2, its KERD is not expected to be identical to that of $EB^{+\bullet}$. Hence, we conclude that PD of $pXL^{+\bullet}$, and other xylene isomeric ions also, proceeds via the same mechanism as in MID.

Rate Constants. To determine the PD rate constants, we recorded the MIKE spectra, or the time-resolved PD-MIKE spectra, such that the photoexcitation and dissociation occur in the presence of an electric field. The time-resolved PD-MIKE profile for the methyl loss of $EB^{+\bullet}$ at 514.5 nm recorded with the electric field of 0.5 kV/cm is shown in Figure 5a. Tailing of the main peak toward the lower translational energy direction occurs because of the time delay between photoexcitation and dissociation. The noisy feature at much lower translational energy (~6870 eV) is due to interference from the MID background. The method to determine the rate constant by analyzing the time-resolved PD-MIKE profile is well established.[15] Briefly, the overall time-resolved PD-MIKE profile is expressed as a weighted sum of $h(K,t)$, which is the peak shape function for the dissociation occurring at time t:

$$H(K) = \int P(t)h(K,t)\,\mathrm{d}t \tag{8}$$

$h(K,t)$ for each t was derived from the shape of the voltage-floated PD-MIKE profile. Here, K is the translational energy scale in the MIKE spectrum. The probability density for dissociation occurring at time t, $P(t)$, may be expressed as below, assuming the random lifetime distribution and the approximately linear relation between log k and E:

$$P(t) \propto \int P(E)k(E)\mathrm{e}^{-k(E)t}\,\mathrm{d}E \propto \int P(\log k)k\mathrm{e}^{-kt}\,\mathrm{d}\log k \tag{9}$$

$P(E)$ is the internal energy distribution for the photoexcited molecular ion. When a Gaussian-type distribution of the internal energy is assumed, the following analytic expression can be used for $P(\log k)$:

$$P(\log k) \propto \exp[-\alpha(\log k - \log k_c)^2] \tag{10}$$

Here, log k_c is the most probable value of log k, and α is a constant related to the width of the distribution. k_c corresponds to the rate constant at the most probable internal energy of the photoexcited ion. k_c and α can be determined by a regression analysis of the experimental time-resolved PD-MIKE profile. The most probable rate constant thus obtained is $(1.6 \pm 0.4) \times 10^8\ s^{-1}$. We also obtained rate constants at other argon ion laser wavelengths, roughly fit the results with the RRKM calculation, and estimated the internal energy range responsible for MID based on the random lifetime assumption,[34] shown as the shaded region in Figure 1.

The time-resolved PD-MIKE profile for the methyl loss of $pXL^{+\bullet}$ at 488.0 nm is shown in Figure 5b. This looks quite different from that of $EB^{+\bullet}$, even though the available energies after photoexcitation are nearly the same in the two cases. The long tail for the dissociation occurring inside the field and the significant intensity of the dissociation occurring after the parent ions exit the field region (~6870 eV) indicate that the dissociation of $pXL^{+\bullet}$ occurs with a smaller rate constant than that of $EB^{+\bullet}$. The best estimate of the PD rate constant for $pXL^{+\bullet}$ obtained by analyzing this profile was $(5 \pm 3) \times 10^6\ s^{-1}$, which is smaller than that of $EB^{+\bullet}$ by a factor of ~30. We also measured the PD rate constants for ortho and meta isomers of the xylene ions at 488.0 nm, which were $(7 \pm 3) \times 10^6$ and $(8 \pm 3) \times 10^6\ s^{-1}$, respectively. The fact that the PD rate constants for all three isomers of the xylene ions are nearly the same means that the rate-determining steps for these reactions occur via the same or energetically similar transition states, as was the case for reactions near the threshold (MID). These rate-determining steps can be either the $XL^{+\bullet} \rightarrow MC^{+\bullet}$ isomerization or $MC^{+\bullet} \rightarrow EB^{+\bullet}$. We could not determine experimentally which of these two steps was rate-determining because the PD experiment for $MC^{+\bullet}$ could not be done. However, considering the results from the analysis of MID-KERDs, it is likely that these rate-determining steps are the isomerization to $MC^{+\bullet}$. The fact that the PD rate constants for $pXL^{+\bullet}$ and $EB^{+\bullet}$ are different can also be explained by difference in the reaction pathways. We ruled out such a possibility based on the KERD data.

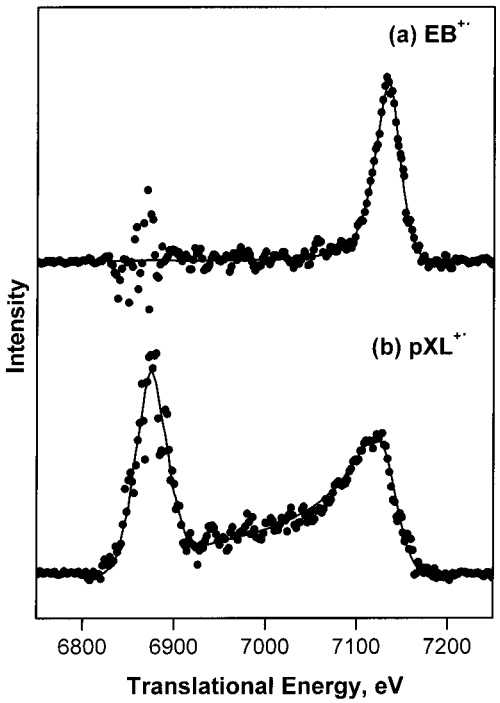

Figure 5. Time-resolved PD-MIKE profiles of $C_7H_7^+$ produced from (a) the ethylbenzene ion at 514.5 nm and from (b) the *p*-xylene ion at 488.0 nm. Experimental and calculated results are shown as solid circles and solid curves, respectively.

The pattern of the time-resolved PD-MIKE profile for $EB^{+\bullet}$, Figure 5a, allows further reasoning on the isomerization processes in Scheme 1. If the isomerization of the photoexcited $EB^{+\bullet}$ to $pXL^{+\bullet}$ can compete with the direct dissociation to $Bz^+ + CH_3^\bullet$, $pXL^{+\bullet}$ thus formed will dissociate slowly, with the rate constant equivalent to its own PD rate constant ($\sim 5 \times 10^6$ s^{-1}). Namely, $pXL^{+\bullet}$ will play the role of a kinetic trap for the excited $C_8H_{10}^{+\bullet}$. Then, the time-resolved PD-MIKE profile for $pXL^{+\bullet}$, Figure 5b, should appear overlapped on the profile in Figure 5a corresponding to faster dissociation. Near absence of the slow dissociation component in Figure 5a, even though excessive noise in the 6900∼7050 eV region in this figure may be attributed to this component, means that the direct dissociation is faster than the isomerization, at least by an order of magnitude. This also allows the following interpretation of the results from the ^{13}C scrambling study[13] of the $C_8H_{10}^{+\bullet}$ systems performed by Grotemeyer and Grützmacher. It was suggested that scrambling of the ^{13}C isotope incorporated in the methyl group of ethylbenzene and methylcycloheptatriene requires efficient forward and backward isomerizations between $MC^{+\bullet}$ and $pXL^{+\bullet}$ in the time scale of dissociation. In the electron ionization spectra of these two compounds, which represent high energy (or fast) dissociations mostly, $^{13}CH_3^\bullet$ was found to be lost preferentially. The present experimental observation that the isomerization cannot compete effectively against the direct dissociation of $EB^{+\bullet}$ in PD is in agreement with the results from the above ^{13}C labeling study. Furthermore, the preferential loss of $^{13}CH_3^\bullet$ was observed not only from $EB^{+\bullet}$ but also from $MC^{+\bullet}$ (∼90% in both cases). This suggests that the $MC^{+\bullet} \rightarrow pXL^{+\bullet}$ isomerization is one of the bottlenecks in the isomerization of the photoexcited $EB^{+\bullet}$ to $pXL^{+\bullet}$. As the internal energy decreases to the level corresponding to the metastable window, the rate constants for the direct dissociations of $EB^{+\bullet}$ and $MC^{+\bullet}$ would decrease more rapidly than that for the isomerization (tight transition state). This will allow conversion of some $EB^{+\bullet}$/$MC^{+\bullet}$ to $pXL^{+\bullet}$ and partial ^{13}C scrambling as observed in MID spectra of $C_8H_{10}^{+\bullet}$ generated from ethylbenzene and methylcycloheptatriene. ^{13}C scrambling would be more extensive as observed in MID of $pXL^{+\bullet}$ because $pXL^{+\bullet} \rightarrow MC^{+\bullet}$ is the rate-determining step in this case.

4. Summary and Conclusions

Production of $C_7H_7^+$ from $C_8H_{10}^{+\bullet}$ ions generated by ethylbenzene; methylcycloheptatriene; and *o*-, *m*-, and *p*-xylenes has been investigated using the MID and PD techniques. Analysis of the KERDs showed that the benzylium (Bz^+)/tropylium (Tr^+) ratios were the same regardless of the precursor ions near the reaction threshold, suggesting rapid interconversion between ethylbenzene ion ($EB^{+\bullet}$) and methylcycloheptatriene ion ($MC^{+\bullet}$) structures. At higher internal energy achieved by photoabsorption, $EB^{+\bullet}$ dissociated to Bz^+ preferentially because either the $EB^{+\bullet} \rightarrow MC^{+\bullet}$ isomerization or the $MC^{+\bullet} \rightarrow Tr^+ + CH_3^\bullet$ could not compete with the direct dissociation of $EB^{+\bullet}$. Even if the isomerization to $MC^{+\bullet}$ occurs rapidly, it is certain that its isomerization to $pXL^{+\bullet}$ hardly occurs, as is evident in the time-resolved PD-MIKE profile of $EB^{+\bullet}$. Also certain is that dissociation of $pXL^{+\bullet}$ near the threshold proceeds via the rate-determining isomerization to $MC^{+\bullet}$. For dissociation of $pXL^{+\bullet}$ at high internal energy, experimental kinetic-energy release data do not support the change in the dissociation pathway to the "H ring-walk" channel. Hence, we conclude that this reaction proceeds via the same mechanism found at the lower internal energy, namely, isomerization to $MC^{+\bullet}$ and then to $EB^{+\bullet}$ followed by dissociation.

The mechanistic picture for the dissociation of the $C_8H_{10}^{+\bullet}$ system presented in this work summarized as Scheme 1 was derived from a detailed analysis of the experimental kinetic energy release distribution and the rate constant. The former was helpful to elucidate the nature of the dissociation steps, whereas the latter was helpful to gain information on the rate-determining steps. This picture is clearly in conflict with the one postulated by Grotemeyer and Grützmacher on the basis of the semiempirical calculation and the ^{13}C labeling study. Calculation of the reaction pathways at higher levels would be useful to interpret the present experimental findings. We have not been successful in this effort yet.

A series of investigations performed in this laboratory for the production of $C_7H_7^+$ from $C_7H_8^{+\bullet}$ (toluene$^{+\bullet}$),[8] $C_8H_{10}^{+\bullet}$ (ethylbenzene$^{+\bullet}$; methylcycloheptatriene$^{+\bullet}$; and *o*-, *m*-, and *p*-xylene$^{+\bullet}$), and $C_9H_{12}^{+\bullet}$ (*n*-propylbenzene$^{+\bullet}$)[10] in MID shows an interesting trend in the variation of the Bz^+/Tr^+ ratio with the total number of carbon atoms in the alkyl groups attached to the ring. The percentage of Bz^+ is ∼17% for the production from $C_7H_8^{+\bullet}$, ∼66% from $C_8H_{10}^{+\bullet}$, and 100% from $C_9H_{12}^{+\bullet}$. Changes in the rate constants for the isomerization and dissociation steps as alkyl groups are added must be responsible for such a variation. Accurate determination of the potential-energy diagrams, especially the energies and structures of the transition states, would be needed to explain this trend.

Acknowledgment. This work was supported financially by CRI, the Ministry of Science and Technology, Republic of Korea. Y.H.K. thanks the Ministry of Education, Republic of Korea, for the Brain Korea 21 fellowship.

References and Notes

(1) Lifshitz, C. *Acc. Chem. Res.* **1994**, *27*, 138.
(2) Buschek, J. M.; Ridal, J. J.; Holmes, J. L. *Org. Mass Spectrom.* **1988**, *23*, 543.
(3) Lifshitz, C.; Gotkis, Y.; Ioffe, A.; Laskin, J.; Shaik, S. *Int. J. Mass Spectrom. Ion Processes* **1993**, *125*, R7.
(4) Bombach, R.; Dannacher, J.; Stadelmann, J.-P. *Chem. Phys. Lett.* **1983**, *95*, 259.
(5) Dunbar, R. C. *J. Am. Chem. Soc.* **1973**, *95*, 472. Shen, J.; Dunbar, R. C.; Olah, G. A. *J. Am. Chem. Soc.* **1974**, *96*, 6227.
(6) Dewar, M. J. S.; Landman, D. *J. Am. Chem. Soc.* **1977**, *99*, 2446.
(7) Cone, C.; Dewar, M. J. S.; Landman, D. *J. Am. Chem. Soc.* **1977**, *99*, 372.
(8) Moon, J. H.; Choe, J. C.; Kim, M. S. *J. Phys. Chem. A* **2000**, *104*, 458.
(9) Smith, B. J.; Hall, N. E. *Chem. Phys. Lett.* **1997**, *279*, 165.
(10) Hwang, W. G.; Moon, J. H.; Choe, J. C.; Kim, M. S. *J. Phys. Chem. A* **1998**, *102*, 7512.
(11) Oh, S. T.; Choe, J. C.; Kim, M. S. *J. Phys. Chem.* **1996**, *100*, 13367.
(12) Stapleton, B. J.; Bowen, R. D.; Williams, D. H. *J. Chem. Soc., Perkin Trans. 2* **1979**, 1219.
(13) Grotemeyer, J.; Grützmacher, H.-Fr. *Org. Mass Spectrom.* **1982**, *17*, 353. Grotemeyer, J.; Grützmacher, H.-Fr. In *Current Topics in Mass Spectrometry and Chemical Kinetics*; Maccoll, A., Ed.; Heyden: London, 1982.
(14) Ausloos, P. *J. Am. Chem. Soc.* **1982**, *104*, 5259.
(15) Lim, S.-H.; Choe, J. C.; Kim, M. S. *J. Phys. Chem. A* **1998**, *102*, 7375. Choe, J. C.; Kim, M. S. *J. Phys. Chem.* **1991**, *95*, 50.
(16) Harrison, A. G.; Honnen, L. R.; Dauben, H. J.; Lossing, F. P. *J. Am. Chem. Soc.* **1960**, *82*, 5593.
(17) Conrow, K. *J. Am. Chem. Soc.* **1961**, *83*, 2343.
(18) Albeck, M.; Tamari, T.; Sprecher, M. *J. Org. Chem.* **1983**, *48*, 2276.
(19) Meyer, F.; Haynes, P.; McLean, S.; Harrison, A. G. *Can. J. Chem.* **1965**, *43*, 211. McLafferty, F. W.; Stauffer, D. B. *The Wiley/NBS Registry of Mass Spectral Data*; Wiley: New York, 1989; Vol. 1, p 65.
(20) Traeger, J. C.; McLoughlin, R. G. *J. Am. Chem. Soc.* **1981**, *103*, 3647.
(21) Lias, S. G.; Bartmess, J. E.; Liebman, J. F.; Holmes, J. L.; Levine, R. D.; Mallard, W. G. *J. Phys. Chem. Ref. Data* **1988**, *17*, Suppl. No. 1.
(22) NIST Standard Reference Database 69, Feb 2000: *NIST chemistry WebBook.*
(23) Baer, T.; Morrow, J. C.; Shao, J. D.; Olesik, S. *J. Am. Chem. Soc.* **1988**, *110*, 5633.

(24) Ellison, G. B.; Davico, G. E.; Bierbaum, V. M.; DePuy, C. H. *Int. J. Mass Spectrom. Ion Processes* **1996**, *156*, 109.

(25) Frisch, M. J.; Trucks, G. W.; Schlegel, H. B.; Scuseria, G. E.; Robb, M. A.; Cheeseman, J. R.; Zakrzewski, V. G.; Montgomery, J. A., Jr.; Stratmann, R. E.; Burant, J. C.; Dapprich, S.; Millam, J. M.; Daniels, A. D.; Kudin, K. N.; Strain, M. C.; Farkas, O.; Tomasi, J.; Barone, V.; Cossi, M.; Cammi, R.; Mennucci, B.; Pomelli, C.; Adamo, C.; Clifford, S.; Ochterski, J.; Petersson, G. A.; Ayala, P. Y.; Cui, Q.; Morokuma, K.; Malick, D. K.; Rabuck, A. D.; Raghavachari, K.; Foresman, J. B.; Cioslowski, J.; Ortiz, J. V.; Stefanov, B. B.; Liu, G.; Liashenko, A.; Piskorz, P.; Komaromi, I.; Gomperts, R.; Martin, R. L.; Fox, D. J.; Keith, T.; Al-Laham, M. A.; Peng, C. Y.; Nanayakkara, A.; Gonzalez, C.; Challacombe, M.; Gill, P. M. W.; Johnson, B. G.; Chen, W.; Wong, M. W.; Andres, J. L.; Head-Gordon, M.; Replogle, E. S.; Pople, J. A. *Gaussian 98*, revision A.6; Gaussian, Inc.: Pittsburgh, PA, 1998.

(26) Unpublished results.

(27) Yeh, I. C.; Kim, M. S. *Rapid Commun. Mass Spectrom.* **1992**, *6*, 293.

(28) Cooks, R. G.; Beynon, J. H.; Caprioli, R. M.; Lester, G. R. *Metastable Ions*; Elsevier: Amsterdam, The Netherlands, 1973.

(29) Holmes, J. L.; Osborne, A. D. *Int. J. Mass Spectrom. Ion Phys.* **1977**, *23*, 189.

(30) Choe, J. C.; Kim, M. S. *Int. J. Mass Spectrom. Ion Processes* **1991**, *107*, 103.

(31) Levine, R. D.; Bernstein, R. B. *Molecular Reaction Dynamics and Chemical Reactivity*; Oxford University Press: New York, 1987. Cho, Y. S.; Choe, J. C.; Kim, M. S. *J. Phys. Chem*. **1995**, *99*, 8645. Lifshitz, C. *Int. J. Mass Spectrom. Ion Phys.* **1982**, *43*, 179.

(32) Chesnavich, W. J.; Bowers, M. T. *J. Am. Chem. Soc*. **1976**, *98*, 8301; *J. Chem. Phys*. **1977**, *66*, 2306; *Prog. React. Kinet*. **1982**, *11*, 137.

(33) Scott, A. P.; Radom, L. *J. Phys. Chem*. **1996**, *100*, 16502.

(34) Robinson, P. J.; Holbrook, K. A. *Unimolecular Reactions*; Wiley-Interscience: New York, 1972.

(35) Nacson, S.; Harrison, A. G. *Int. J. Mass Spectrom. Ion Processes* **1985**, *63*, 325.